GT2006-90283

TEST RESULTS AND ANALYTICAL PREDICTIONS FOR ROTOR DROP TESTING OF AN AMB EXPANDER/GENERATOR

Lawrence Hawkins, Alexei Filatov, Shamim Imani
Calnetix, Inc., Cerritos, CA 90703, USA

Darren Prosser
Air Products, Allentown, PA USA

ABSTRACT

A cryogenic gas expander system that incorporates a high performance, high-speed permanent magnet, direct-drive generator and low loss magnetic bearings is described. Flow loop testing to 30,000 rpm was completed at the system manufacturer's facility in January 2005, and field installation is scheduled for October 2005. As part of the system testing, the rotor was dropped onto the backup bearings multiple times at an intermediate speed and at 30,000 rpm. Orbit and time-history data from a full speed drop and spin down are presented and discussed in detail. A transient, nonlinear rotordynamic analysis simulation model was developed for the machine to provide insight into the dynamic behavior. The model includes the dead band clearance, the flexible backup bearing support and hard stop. Model predictions are discussed relative to the test data.

INTRODUCTION

A direct drive expander/generator on active magnetic bearings (AMBs) has recently been developed which has the high-speed expansion turbine directly mounted onto the generator shaft. Expanders have been used for some time to provide refrigeration in industrial air separation plants. When the shaft energy is greater than 100 kW, economics have allowed energy recovery by driving a 50-60 Hz generator through a gearbox. The new system eliminates gearbox, maintenance, and support systems and allows economic energy recovery down to 10 kW. Furthermore, by incorporating AMBs, the system becomes a completely oil-free system that reduces the risk of accidental contamination of the process. The expander/generator module is shown in Fig. 1 with the nominal

114 mm (4.5 inch) expander wheel used for the initial prototype application. Up to 110 kW of refrigeration power will be consumed by the prototype expander which will be placed into service in an air separation plant in Europe. The expander/generator utilizes a permanent magnet (PM) generator and magnetic bearings contained within a high-pressure-capable housing. The generator has a conventional tooth type stator together with a two pole, high strength steel sleeved rotor assembly. This arrangement is configured for minimum rotor losses and the cold temperatures the rotor may see in the cryogenic expansion process. The expander/generator rotor is supported by two PM bias, radial AMBs and an anisotropic (load capacity in one direction is larger than the other direction), electromagnetic (EM) bias axial AMB. A duplex pair of angular contact backup bearings is located on each end of the machine.

The overall system design of the generator module, including the control system, and rotordynamics were discussed in Hawkins [1]. The design of the magnetic bearing actuators was described in Filatov [2]. A necessary component of a magnetic bearing system for turbomachinery rotors is an auxiliary or backup bearing system. Backup bearings are typically ball bearings, but bushings are also sometimes used in low cost, lightweight machines. The backup bearings provide support for the rotating assembly when the magnetic bearing system is deactivated. Also, in the event of a failure of some component of the magnetic bearings or in the event of an overload of the magnetic bearings, the backup bearings provide rotor support. In normal operation, the backup bearings are not active as they will have a small radial clearance to the rotating assembly. This clearance is typically less than one-half of the magnetic bearing air gap. The backup bearings in this machine, duplex pairs of angular contact ball bearings, are supported in resilient mounts with a hard stop to limit radial deflection.
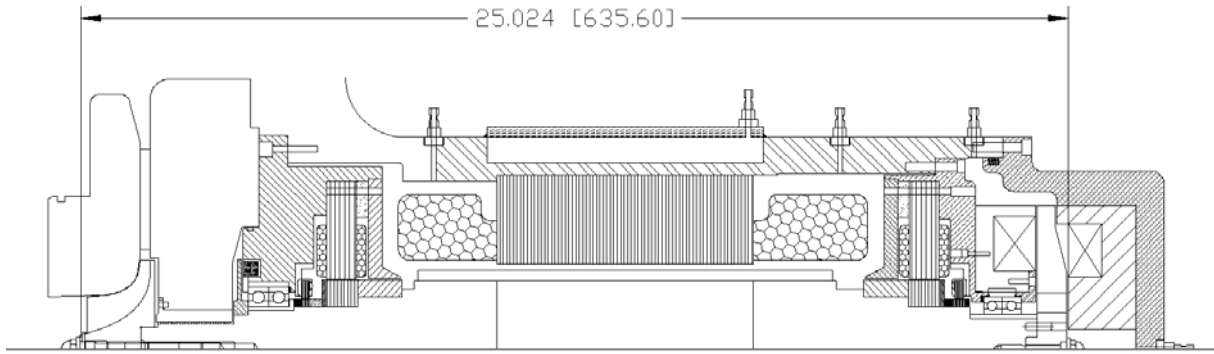
Figure 1. Cross-section of expander generator with nominal 114 mm (4.5 in) wheel.

A typical certification test for a backup bearing system is to intentionally deactivate the magnetic bearings at operating speed, causing the rotor to drop onto the backup bearings and spin down to rest. There is a substantial body of work in the open literature that investigates the dynamics of AMB rotors in backup bearings. Kirk [3] presented a detailed nonlinear analysis for a rotor dropped into backup bearings. Hawkins [4] developed a rotordynamic simulation that included a nonlinear magnetic bearing saturation model as well nonlinear backup bearing clearance effects to analyze shock response in a magnetic bearing system. Cuesta [5] presented a analysis that included a kinematic impact model and compared the predictions to test data on a small test rig. Keogh [6] has been studying control schemes that improve magnetic bearing performance during auxiliary bearing contact due to temporary overload. Several authors have described full five axis drop tests for test rigs or for machines intended for industrial service. Kirk [7] and Swanson [8] have presented numerous test results and analysis from a full scale, AMB rotor drop test stand. Schmeid and Pradetto [9] presented drop test results for a 8.9 kN (one ton) compressor rotor. Caprio [10] presented results for drop testing on a large, vertical energy storage flywheel. However, all of these drop tests are for machines considerably heavier and slower than the expander/generator described here, and all but [10] are for EM bias magnetic bearings. The backup system for the new expander/generator was tested by completing 10 full drops and spin-downs from 23,000 rpm and 10 full drops and spin downs from 30,000 rpm. Position orbit data and time history data from one of the full speed drops are presented here. A nonlinear simulation analysis was developed to help interpret the results and to estimate the loads reacted by the backup bearings. The results of this analysis are discussed relative to the test data.

BACKUP BEARING DESIGN

The backup bearing system for the expander generator consists of two pairs of duplex, face-to-face, angular contact ball bearings. The bearing pair on the expander end of the machine provides backup in both thrust and radial directions (Fig. 2). Both bearing pairs had a light preload, factory set by grinding the inner and outer race end faces to achieve a precise offset which results in a preload when the bearing pair is locked together. The key parameters for the backup bearing design are summarized in Table 1. The bearings are hybrid ceramic, with conventional SAE 52100 steel races and SiN3balls. Brass landing sleeves on the rotor provide a non-sparking touchdown surface on the shaft, a requirement for some of the potential applications of the generator/expander unit. The radial backup bearing clearance is nominally 0.09 mm (0.0035 in). The clearance is atypically small, 17.5% of magnetic air gap, to accommodate clearance requirements of the expander wheel. Both backup bearing pairs are mounted in a resilient mount which reduces the support stiffness to 1.3E7 N/m (75,000 lbf/in). Compliance in the machined metal mount is achieved using tangential spring arms that have a slip fit into the housing. The mount is intended to serve several purposes: 1) reduce the synchronous reaction forces during a critical speed traverse (by lowering the forward natural frequency), 2) reduce the impact force during a drop down event, and 3) reduce the whirl frequency (by lowering the lowest support natural frequency).
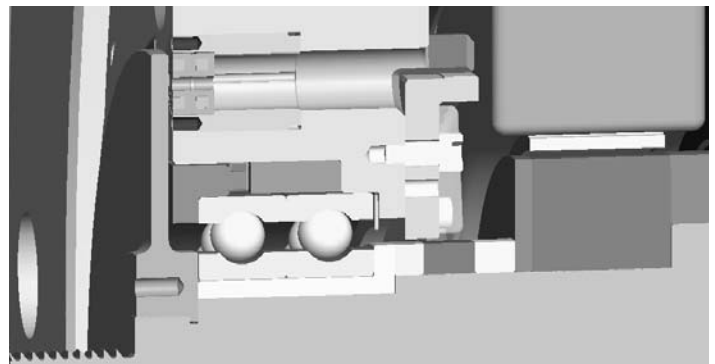
Figure 2. Cross-section showing radial/thrust backup bearing.

The resilient mount also contributes light friction damping through slipping at the interfaces of the mount and the housing. The requirements listed above drive the design toward low stiffness values; however, the lower bound on stiffness is set by the maximum radial displacement allowed by critical clearances in the machine. In particular, peak deflection during the drop or impact transient must be considered as well as the static sag on the backup bearings. This is particularly important in turbomachinery where it is desired to keep design clearances between the impeller and shroud as small as possible.

Table 1. Rotor and backup bearing parameters.

Nominal Spin Speed, rpm	30,000
Rotor Mass, kg (lbm)	29.0 (63.9)
Polar Inertia, kg-m^2 (lbm-in^2)	0.039 (133)
Trans Inertia, kg-m^2 (lbm-in^2)	0.718 (2448)
Distance from Expander End Backup Brg to CG, mm (in)	251 (9.90)
Backup Bearing Span, mm (in)	472 (18.59 in)
AMB Passive Negative Stiff, each brg, N/m (lbf/in)	1.93E6 (11,000)
Bearing bore, mm Expander End Non-expander End	55 45
Bearing preload, N (lbf) Expander End Non-expander End	315 (71) 230 (52)
Backup Brg Rad Clr, mm (in)	0.09 (0.0035)
Resilient Mount Stiffness, N/m (lbf/in)	1.3E7 (75,000)
Hard Stop Rad Clr, mm (in)	0.127 (0.005)
Rotor Sleeve Material	Lead Bronze

In this machine, the allowable travel on the resilient mount is restricted to a minimum of 0.038 mm (0.0015 in) radial. Beyond that, the resilient mount is bypassed by contact between the bearing outer race and the housing, resulting in the much stiffer support stiffness of the duplex bearing pair in series with the housing. A design choice was made to set the minimum stiffness for the resilient mount by limiting the static sag to half of the minimum travel, or 0.019 mm (0.00075 in). This sets a lower bound on stiffness of 7,900 N/mm (45,000 lbf/in) at each end of the machine for the 29 kg (64 lbf) rotor. The support stiffness from the mount is somewhat asymmetric, having the same stiffness in orthogonal axes, but a softer value in between. The influence of equivalent backup bearing stiffness on the critical speeds is shown by the undamped critical speed map in Fig. 3. The analysis includes constant values for the permanent magnet bias negative stiffness at the magnetic bearing actuator locations. With the target mount stiffness of 1.3E7 N/m, the lowest rigid body critical speed is 8,000 rpm (133 Hz).
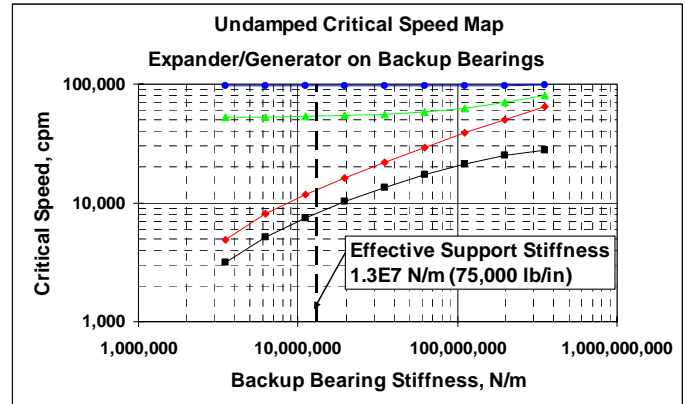
Figure 3. Undamped critical speed map for the rotor supported at the backup bearings.

BACKUP BEARING ROTOR DROP TESTING

The backup system was tested by completing 10 full drops and spin-downs from 23,000 rpm and 10 full drops and spin downs from 30,000 rpm (full speed). All of the drop transients are of short duration, because the system control is configured to brake the rotor quickly to rest in the event of an alarm condition. This is done by closing the inlet slam valve to the expander, thus removing the driving source. The generator is then loaded with a resistor bank located in the control cabinet which pulls the machine speed from 30,000 rpm to rest in about 10 seconds.

The position data from one of the 30,000 rpm drops is shown in Figs. 4 - 6. The data was collected by the logging feature of the magnetic bearing controller. This feature automatically writes position sensor and current command data to synchronous RAM when triggered by a delevitation or an alarm condition. The position sensors are between the magnetic bearings and backup bearings and provide a good estimate of the relative shaft/housing motion at the backup bearings. The radial bearing (and sensor) axes are oriented at 45 degrees to the vertical to share gravity load between the two bearing axes. The configuration of the data acquisition, which was set up to accommodate a wide range of needs during commissioning, allowed a data set length of 6 seconds at a 1750 Hz sample rate. Although this sample rate is somewhat marginal for recording synchronous motion, it provides excellent fidelity for the largely rigid body motions during the rotor drop.

Figure 4 shows the radial displacement amplitude at the expander end bearing and the spin speed versus time. Considering the radial position data, the delevitation event occurs at about 1.28 seconds (there is a 1.28 second pre-trigger on the data acquisition). The speed drops slightly due to the added drag from the backup bearings and then recovers. The slam valve closes at about 2.5 seconds, removing the driving source and allowing the generator to pull the speed down to zero. The delay between the drop and the shutdown occurs because the drive enable (alarm) signal from the magnetic

bearing has a 1.0 second delay to avoid nuisance trips. The 6 second record length setting for the internal data acquisition allowed data recording only down to 16,000 rpm.

Orbit plots for three different time slices are shown in Fig. 5. The positive coordinate axes are 45° to either side of the vertical. The time slice from 1.28 – 1.43 seconds, Fig. 5a, shows the drop transient. After hitting the backup bearing, the rotor bounces several times while staying in roughly the same spot on the bearing. The bearing inner race should be spinning up toward the rotor speed during this period. Just after 1.43 seconds the rotor goes into a whirl for about 0.4 seconds as shown in the time slice from 1.43 - 1.83 seconds (Fig. 5b). This whirl motion is somewhat elliptical due to the asymmetry of the resilient mount. The rotor then settles down to a rocking oscillation at the bottom of the backup bearing for the remainder of the time record (1.83 – 6 seconds shown in Fig. 5c). In several other drop tests (data not shown), the rotor took on a rocking motion at the bottom of the bearing just after the initial drop, followed by the same short duration circular whirl observed in Fig. 5b.
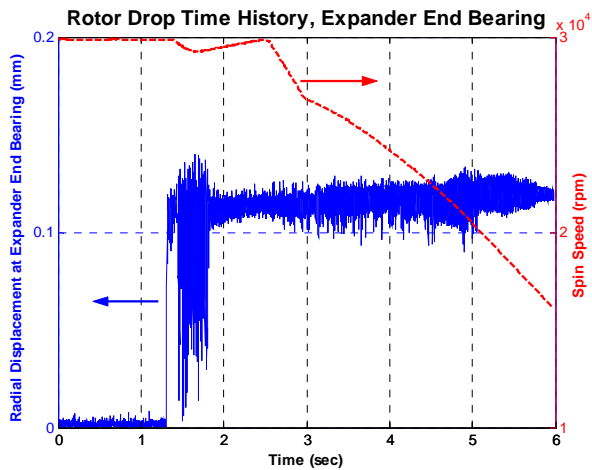
Figure 4. Displacement and speed vs. time during rotor drop and spin down.

Expanded time histories from the orthogonal x and y position sensors are shown in Figs. 6. The rotor spin vector is along the positive z coordinate so for forward circular whirl, x would lead y by 90°. Figure 6a shows the time history data from 1.28 to 1.43 seconds. From this perspective it can be seen that the rotor bounces at about 125 Hz after it hits the backup bearing. Figure 6b shows the time slice from 1.4 to 1.6 seconds when the rotor is executing a roughly circular whirl around the backup bearing clearance space. The whirl is forward whirl as the x signal leads the y signal. Forward whirl observations have been reported by numerous authors [5,8-10]. The x signal clearly has a longer period on the positive half cycles compared to the negative half cycles. This probably happens because in the negative direction, the combined static weight and dynamic load compress the resilient mount to the hard (stiff) stop. In the positive direction, the spring is not fully compressed and the

(a)

(b)

(c)
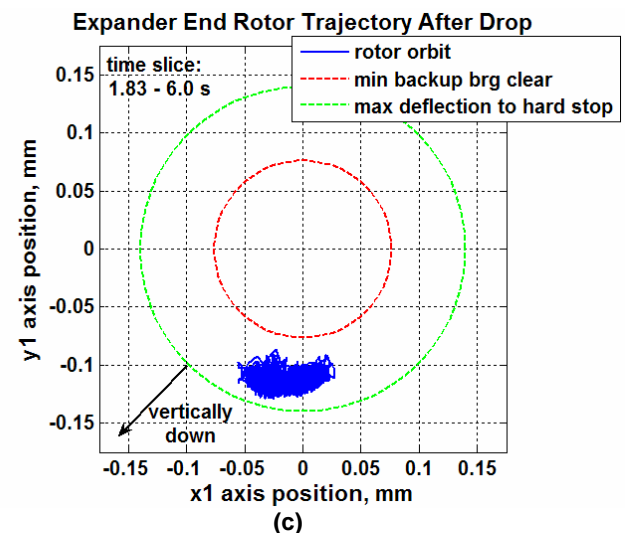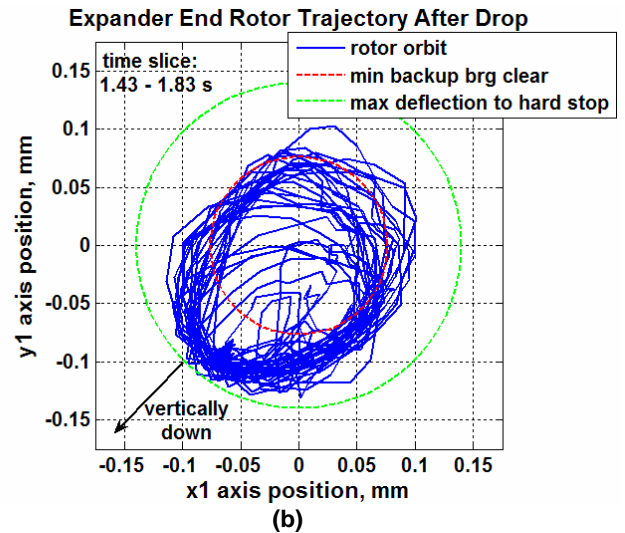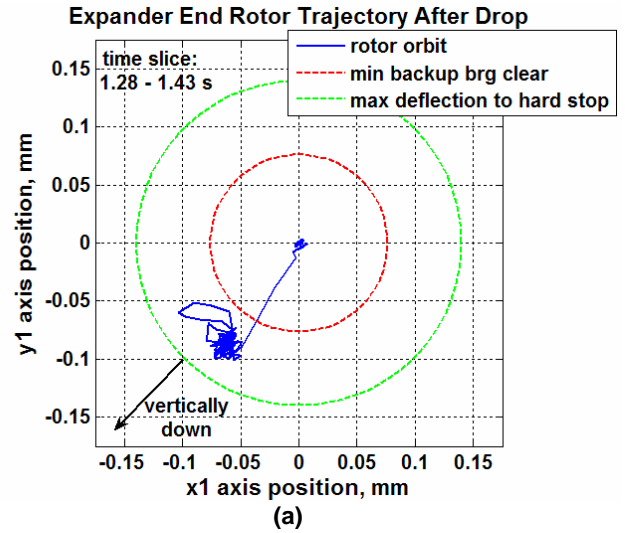
Figure 5. Displacement orbit at expander end during rotor drop and spin down.

rotor spends part of the cycle in the clearance space. A Fourier transform of the signal during the full whirl shows the dominant frequency is 82 Hz, with a much smaller 110 Hz component.

Figure 6c shows a time slice from 3.2 to 3.9 seconds during the spin down when the rotor was rocking at the bottom of the backup bearing. In this time slice the rocking frequency is initially 50 Hz and then switches to about 110 Hz around 3.7 - 4.0 seconds when the rotor speed is near 24,000 - 22,000 rpm. At lower speeds, the rotor seemed to switch back and forth periodically between and 50 Hz and 110 Hz. The 50 Hz motion can be explained by assuming that the rolling element bearings allow the rotor rigid body to effectively slip along the arc of the backup bearing inner race. This is the motion of a simple pendulum which for a small rocking angle has a natural frequency, fn of:

$$f_n = \sqrt{\frac{g}{r}} \ \frac{1}{2\pi} \ Hz \qquad (1)$$

where g is the gravitational constant (9.81 m/s^2) and r is the radius of the rocking motion. Given that the effective rocking radius, the backup bearing clearance plus static deflection, is about 0.11 mm (0.0042 in), Eq. 1 predicts a natural frequency of 48 Hz, very close to the measured value. It is possible that the 110 Hz motion is due to a rocking mode with the two ends of the rotor out-of-phase, however, the data show a phase difference of less than 45° between the two end of the rotor throughout the spin down. It is more likely that the 110 Hz is a transient response of the lowest rigid body mode of the rotor on the resilient mounts.

After completion of testing, the bearings were disassembled and inspected and found to be in reusable condition. There was no evidence of Brinell damage that would have indicated excessive impact loading. The measured hardness values for the races were within factory specification of 58.5–61 Rockwell C, indicating that the races temperatures stayed well below the 204°C (400 °F) annealing threshold. There was evidence of minor slipping on the races of the inboard bearing of the expander end pair. This bearing can be unloaded during a touchdown if the thrust load is high enough. Higher preload could prevent this but was traded off against margin for thermal growth in the design.

NONLINEAR ROTOR DROP SIMULATION

A nonlinear, simulation model for the rotor/housing/backup bearing system was developed to investigate several aspects of the data and the design, and to determine: 1) the bearing loads during the whirling and rocking phases of the motion, and 2) the influence of rotor balance quality on the rocking and whirling motions. The simulation was performed using an analysis tool previously described [4]. In this analysis, the rotordynamic
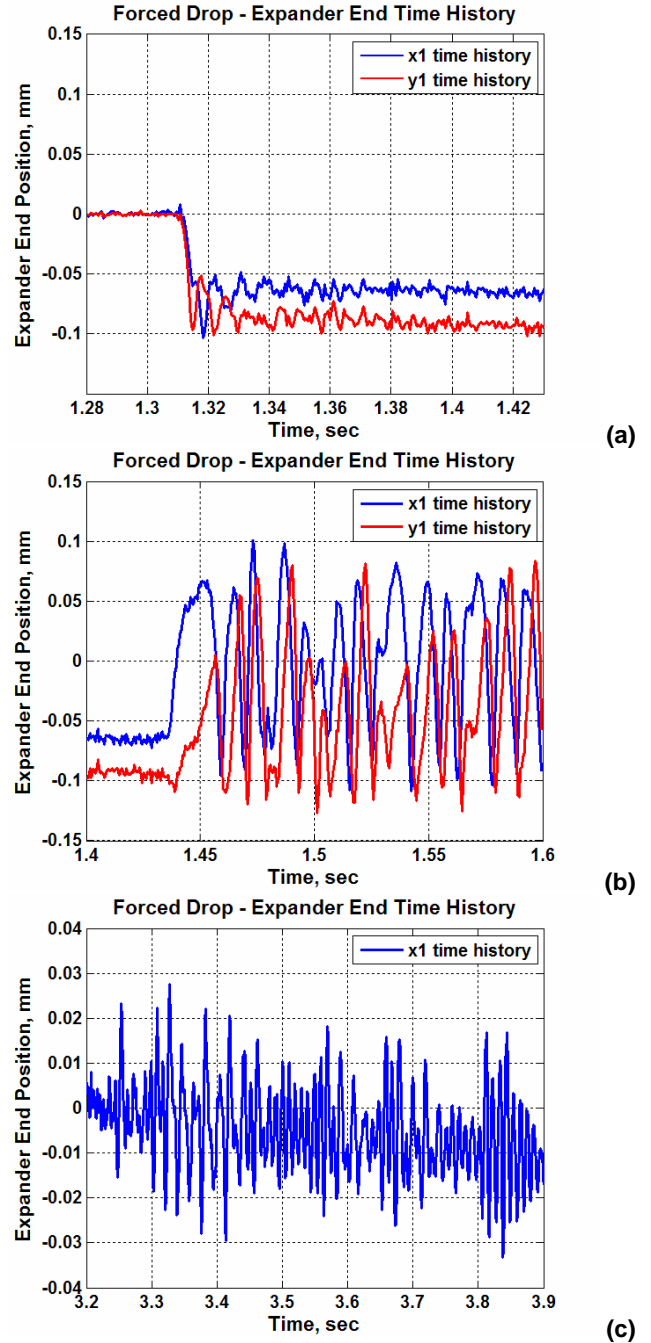
Figure 6. Displacement time history at expander end.

equations of motion for a coupled rotor/casing system represented in second order form are:

$$[M]\{\ddot{q}\} + [C]\{\dot{q}\} + [K]\{q\} = \{f\} \qquad (2)$$

where M, C, K, represent the mass, damping and stiffness matrices for a coupled rotor housing system, and q is a vector of physical displacements. Nonlinear and time dependent forces are applied as part of the external force vector, f.

Equation 2 is integrated through time using the Newmark-β algorithm. This formulation allows simulation modeling of backup bearings with large clearance, friction during inner race spinup, bearing mount flexibility, and a hard stop to limit radial displacement on the mount. This approach has been used extensively by the author to model rotor drop events onto backup bearings.

A weakness of the simulation tool is that it does not currently have a sophisticated impact contact model; therefore it cannot be used to make accurate estimates of loads and dynamics just after impact. Therefore, the focus of the simulations reported here is on other aspects of the backup bearing drop. This is not to minimize the importance of the drop transient as drop impact loads can be large enough to cause Brinnell damage and early failure, particularly in machines with hard mounted backup bearings. Resiliently mounting the backup bearings, as in the expander/generator studied here, will reduce the impact loads. As mentioned above, the post test inspection of the bearings showed no impact damage.

The system model that was created included the flexible rotor model, an axisymmetric housing model that provides a good approximation of the total mass and mass distribution of the housing, a backup bearing model, and the magnetic bearing. The housing was connected to ground at the impeller end mounting flange using vertical and horizontal shear and moment springs. The spring values were selected so that the lowest measured natural frequencies (85 Hz horiz. and 195 Hz vertical) were predicted. The nominal bearing model includes a 0.09 mm (0.0035 in) radial clearance space, a linear stiffness of 1.3E7 N/m (75,000 lbf/in), and no tangential friction between the bearing inner race and the shaft. A hard stop in parallel with the resilient mount has a radial clearance space of 0.127 mm (0.005 in) and stiffness of 8.8E7 N/m (500,000 lbf/in). The magnetic bearings were included in the model for preliminary runs to establish initial conditions for the drop analysis. Those initial conditions are used for all of the simulation runs reported here, but the magnetic bearing control force is zeroed at the beginning of the run, so the rotor drop occurs at time zero ($t = 0$ seconds) for all reported results. The magnetic bearing actuators used in this machine have a permanent magnet bias so the passive radial negative stiffness of 1.9E6 N/m (11,000 lbf/in) per bearing remains in the model at the magnetic bearing actuator locations even after the drop. The nominal unbalance was 12.7 gm-mm (0.5 gm-in) at the impeller and 25.4 gm-mm (1.0 gm-in) at the axial magnetic bearing disk. The static weight of the rotor (285 N/63.9 lbf) and housing (6681 N/1498 lbf) are applied as separate distributed loads calculated by multiplying the mass matrix by the gravitational acceleration constant. Gravity acts in the negative y direction in the model.

Figures 7-10 show predicted results for rotor drop simulations at a spin speed of 30,000 rpm. The presented results are all for the expander end touchdown bearing. The displacement orbit during and after the drop for the nominal model is given in Fig. 7a. The rotor bounces a number of times

(a)

(b)

(c)
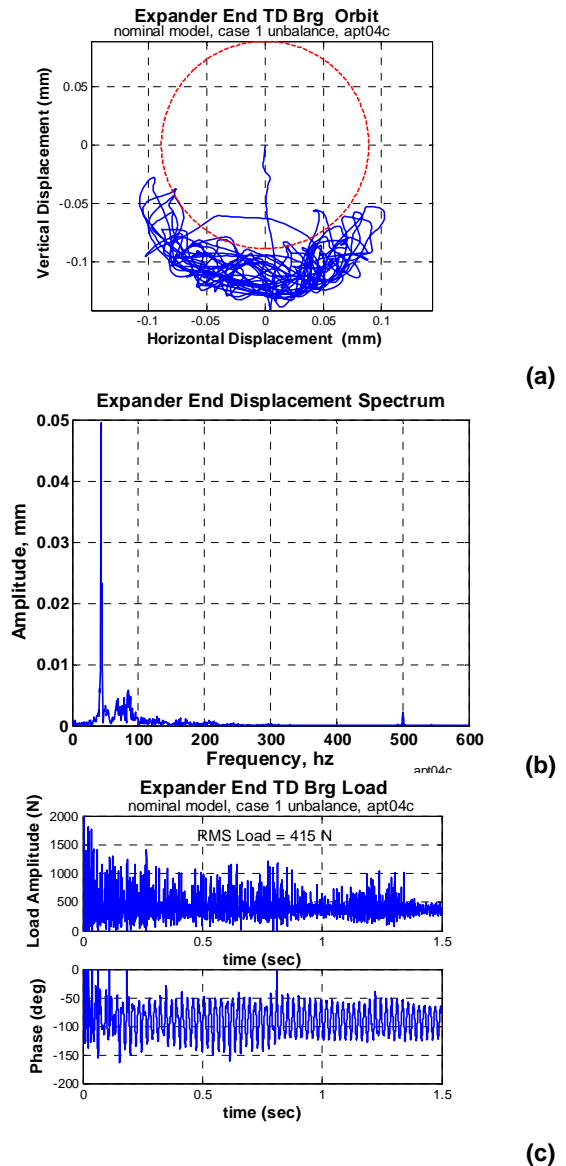
Figure 7. Predicted drop response for nominal model: a) orbit at expander end, b) Fourier transform of x axis, c) expander end backup brg load mag and phase.

and then settles into a rocking motion covering about 110 degrees at the bottom of the bearing. This behavior is a reasonable simulation of the actual rotor motion in its rocking phase (see Fig. 5c). The Fourier transform of this motion in Fig. 7b shows that the motion is mostly at 45 Hz, with much smaller response at 90 Hz and the 500 Hz spin frequency. The 45 Hz motion is in good agreement with the measured data and the fundamental pendulum calculation in Eq. 1. The bearing load magnitude and phase, Fig. 7c, show that the load has a number of impact peaks up to 1784 N (400 lbf), but is generally below 446 N (100 lbf). The RMS value of the load is 415 N (93 lbf). This predicted load is shared between the duplex bearing pair, and is carried largely by the resilient mount, with the hard stop coming into play intermittently.

In order to investigate the loads in a whirling condition, additional unbalance was added to the rotor model in several steps. Other authors [5,7] have suggested that the tendency to full whirl should increase as the unbalance force approaches the rotor weight. The unbalance values used and the subsequent ratio of unbalance to the rotor weight at 30,000 rpm are given in Table 2, where G = rotor weight (285 N). The unbalance force is a vector sum of the two applied unbalances. Unbalance is applied at the impeller and thrust disk because those two components were balanced as components and installed on the balanced generator rotor. The nominal unbalance, Case 1, reflects the estimated unbalance based on operation on the magnetic bearings. The additional unbalance for Cases 2-4 was added to the thrust disk because this component is significantly heavier than the impeller and would produce the largest unbalance from relocation error.

Table 2. Unbalance Cases

Case	Unbalance (gm-mm)		G @ 30 krpm
	Impeller (0°)	Thrust Disk (90°)	
1	12.7	25.4	0.98
2	12.7	50.8	1.81
3	12.7	127.0	4.42
4	12.7	254.0	8.81

Figure 8 shows the predicted displacement orbit for unbalance Case 2. The rotor still rocks at the bottom of the bearing, but the rocking motion now approaches a 180 degree arc. The rocking frequency is still dominated by 45 Hz, but there is also a significant component at 90 Hz. The predicted orbit for unbalance Case 3, Fig. 9, shows the rotor bouncing in and out of the clearance space, occasionally executing full whirl cycles. The dominant frequency is 125 hz which is approximately the expected lowest rigid body mode on the resilient mount. The result for the largest analyzed unbalance, Case 4, is shown in Fig. 10. The predicted whirl orbit predominately circles the clearance space, with occasional excursions into the clearance space. The dominant frequency is 130 Hz and there is a substantial component at the 500 Hz spin frequency. These results certainly indicate that increasing the level of unbalance pushes the rotor from a rocking orbit to a full orbit. To predict the threshold of whirl, additional unbalance cases were run where the unbalance was progressively increased from the Case 2 value. An unbalance level of 1.95 G was required before the simulation began predicting full whirl. The predicted whirl threshold so much greater than 1.0 G must be partly due to the permanent magnet negative stiffness. With the rotor at the bottom of the backup bearing the additional downward force from the negative stiffness is slightly greater than the rotor weight (1.2 G). In a simulation using the Case 2 unbalance with no negative stiffness, a larger angle rocking motion was predicted

compared to Fig. 8, but full whirl still was not predicted. Additional factors are; 1) that most of the unbalance is applied at the end of the rotor, at the thrust disk, instead of at the center-of-gravity, 2) relative proximity of the spin frequency to system natural frequencies should impact the onset of the whirl condition.
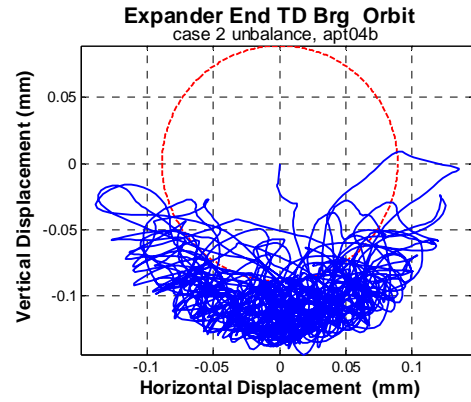
Figure 8. Predicted displacement orbit for unbal Case 2.
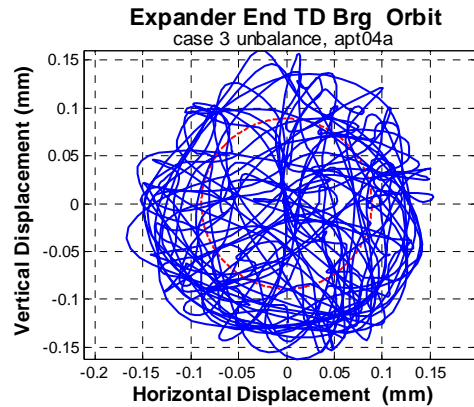
Figure 9. Predicted displacement orbit for unbal Case 3.
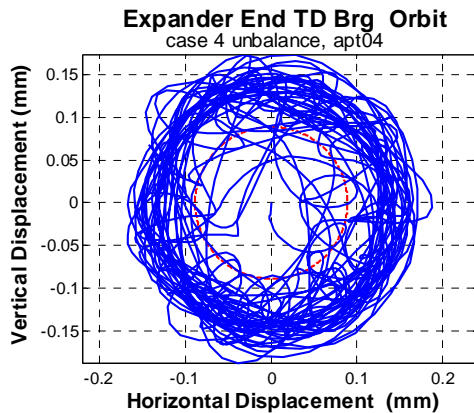
Figure 10. Predicted displacement orbit for unbal Case 4.

The loads predicted for the different unbalance cases are summarized in Table 3. The RMS load certainly increases as the rotor approaches full whirl, but this would happen with these changes in balance quality even without the large clearance space. Even with the worst balance case analyzed, the predicted loads are not unreasonable for the duplex pair of backup bearings. However, a correlation of the observed synchronous orbit on magnetic bearings with the rotordynamic model suggests that it is unlikely that the balance quality relative to the backup bearing journals is any worse than the milder Case 2 unbalance. Additional simulations show that for the Case 3 and Case 4 unbalance, the full whirl should be sustained down to about 5,000 rpm. So it is not clear what causes the rotor to execute a brief forward whirl sometime after the initial drop followed by a return to a rocking motion. In some simulation runs, a coefficient of friction of 0.1 was included at the inner race/shaft contact point to try to produce whirl at a lower unbalance level, but there was not a substantial change in the result. Two other factors that might affect the whirl behavior that may not be well characterized in the simulation are support stiffness asymmetry and damping or other energy dissipation factors.

Table 3. Predicted Loads for Different Unbalance Cases.

Case	RMS Load N (lbf)	Peak Load N (lbf)
1	415 (93)	1784 (400)
2	455 (102)	2230 (500)
3	1227 (275)	6690 (1500)
4	2163 (485)	9812 (2200)

CONCLUSIONS

Backup bearing rotor drop testing was successfully conducted for an AMB supported expander/generator. The test results were presented and discussed. Results from a nonlinear simulation of the drops were presented and discussed.

1) The measurements show a brief period of forward whirl, shortly after touchdown, followed by a rocking motion at the bottom of the backup bearings during the spin down.
2) The simulation analysis shows that as the unbalance level increases, the expected rotor motion in the backup bearings should transition from a rocking motion to full whirl. This doesn't seem to explain the brief full whirl of the rotor in this machine, since the simulation predicts that full whirl motion should be sustained down to 5,000 rpm, whereas the data show only a brief whirl period. Weaknesses in characterizing unbalance distribution, stiffness asymmetry, and energy dissipation factors in the simulation model may be at fault.

3) The simulation predicts that the bearing reaction loads do not go up in a marked way after transition from rocking to full whirl, other than that implied by the increased unbalance.
4) The measured rocking frequency of 50 Hz is correctly predicted by assuming the rocking motion is the motion of simple pendulum. The nonlinear simulation also predicts the same rocking frequency for a well balanced rotor.

REFERENCES

[1] Hawkins, L., Imani, S., Prosser, D., Johnston, M., 2004, "Design and Shop Testing of a 165 kW Cryogenic Expander/Generator on Magnetic Bearings," Proc. 9th Int. Symp. Magnetic Bearings, Paper 60, Lexington, KY.
[2] Filatov, A., McMullen, P., Hawkins, L., Blumber, E., 2004, "Magnetic Bearing Actuator Design for a Gas Expander Generator," Proc. 9th Int. Symp. Magnetic Bearings, Paper 81, Lexington, KY.
[3] Kirk, R.G., Raju, K.V.S., Ramesh, K., 1997, "Modeling of AMB Turbomachinery for Transient Analysis," Proc. MAG 97, Alexandria, VA, pp. 139-153.
[4] Hawkins, L. A., 1997, "Shock Analysis for a Homopolar, Permanent Magnet Bias Magnetic Bearing System," ASME Turbo Expo Paper 97-GT-230, Orlando, FL.
[5] Cuesta, E.N., Montbrun, N.I., Rastelli, V., Diaz, S.E., 2005, "Simple Model for a Magnetic Bearing System Operating on the Auxiliary Bearing" ASME Turbo-Expo Paper GT-2005-69013, Reno-Tahoe, NV.
[6] Keogh, P., Cole, M., Sahinkaya, N., Burrows, C., 2002, "On the Control of Synchronous Vibration in Rotor/Magnetic Bearing Systems Involving Auxiliary Bearing Contact," ASME Turbo-Expo Paper GT-2002-30292, Amsterdam The Netherlands.
[7] Kirk, R. G., Swanson, E. E., Kavarana, F. H., Wang, X., Keesee, J., 1994, "Rotor Drop Test Stand for AMB Rotating Machinery, Part I: Description of Test Stand and Initial Results," Proc. 4th Int. Symp. Magnetic Bearings, ETH Zurich, pp. 207-212.
[8] Swanson, E. E., Kirk, R. G., Wang, J., 1995, "AMB Rotor Drop Initial Transient on Ball and Solid Bearings," Proc. MAG 95, Alexandria, VA, pp. 207-216.
ETH Zurich, pp. 207-212.
[9] Schmied, J. and Pradetto, J.C., 1992, "Behavior of a One Ton Rotor Being Dropped into Auxiliary Bearings," Proc. 3rd Int. Symp. Magnetic Bearings, Alexandria, VA, pp. 145-156.
[10] Caprio, M. T., Murphy, B. T., Herbst, J. D., 2004, "Spin Commissioning and Drop Tests of a 130 kW-hr Composite Flywheel," Proc. 9th Int. Symp. Magnetic Bearings, Paper 65, Lexington, KY.